

# **Drag Measurements on Long, Thin Cylinders at Small Angles and High Reynolds Numbers**

**William L. Keith  
Kimberly M. Cipolla  
David R. Hart  
NUWC Division Newport**

**Deborah A. Furey  
NSWC Division Carderock**



**Naval Undersea Warfare Center Division  
Newport, Rhode Island**

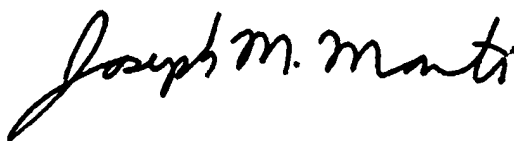
## **PREFACE**

This report was prepared under Project No. TD2115, "Towed Systems Tracking Through Turns," principal investigator William L. Keith (Code 15242). The sponsoring activity is the Office of Naval Research, program managers James McEachern (ONR-321MS) and Ronald Joslin (ONR-333).

The technical reviewer for this report was Michael R. Williams (Code 15242).

The authors acknowledge the additional funding support of Richard B. Philips under the NUWC Division Newport In-House Laboratory Independent Research (ILIR) Program, Project No. D623004, "Investigation of Boundary Layer Development on Small Diameter Towed Arrays," principal investigator Kimberly M. Cipolla (Code 15241).

**Reviewed and Approved: 15 July 2004**



**Joseph M. Monti**  
**Head, Sensors and Sonar Systems Department**



REPORT DOCUMENTATION PAGE			Form Approved OMB No. 0704-0188	
Public reporting for this collection of information is estimated to average 1 hour per response, including the time for reviewing instructions, searching existing data sources, gathering and maintaining the data needed, and completing and reviewing the collection of information. Send comments regarding this burden estimate or any other aspect of this collection of information, including suggestions for reducing this burden, to Washington Headquarters Services, Directorate for Information Operations and Reports, 1215 Jefferson Davis Highway, Suite 1204, Arlington, VA 22202-4302, and to the Office of Management and Budget, Paperwork Reduction Project (0704-0188), Washington, DC 20503.				
1. AGENCY USE ONLY (Leave blank)		2. REPORT DATE 15 July 2004		3. REPORT TYPE AND DATES COVERED
4. TITLE AND SUBTITLE  Drag Measurements on Long, Thin Cylinders at Small Angles and High Reynolds Numbers			5. FUNDING NUMBERS	
6. AUTHOR(S)  William L. Keith Kimberly M. Cipolla David R. Hart Deborah A. Furey				
7. PERFORMING ORGANIZATION NAME(S) AND ADDRESS(ES)  Naval Undersea Warfare Center Division 1176 Howell Street Newport, RI 02841-1708			8. PERFORMING ORGANIZATION REPORT NUMBER  TR 11,555	
9. SPONSORING/MONITORING AGENCY NAME(S) AND ADDRESS(ES)  Office of Naval Research 800 North Quincy Street Ballston Tower One Arlington, VA 22217-5660			10. SPONSORING/MONITORING AGENCY REPORT NUMBER	
11. SUPPLEMENTARY NOTES				
12a. DISTRIBUTION/AVAILABILITY STATEMENT Approved for public release; distribution is unlimited.			12b. DISTRIBUTION CODE	
13. ABSTRACT (Maximum 200 words)  Measurements of the drag caused by turbulent boundary layer mean wall shear stress on cylinders of aspect ratio $L/a = 480$ and $960$ at varying small angles of attack to the tow direction and at length Reynolds numbers of $8 \times 10^6 < Re_L < 6 \times 10^7$ are presented. The use of a full-scale, high-speed towing tank allowed turbulent boundary layers to be developed on cylinders made of either stainless steel, aluminum, titanium, or polyvinyl chloride. The diameter of all cylinders in this experiment was 12.7 mm; two cylinder lengths, 3.05 m and 6.10 m, were used. The use of materials of various densities allowed critical angle tows, resulting in linear cylinder geometry for tow speeds ranging from 2.6 to 20.7 m/s and angles between $0^\circ$ and $12^\circ$ . Towing angles were measured with digital photography, and streamwise drag was measured with a strut-mounted load cell at the tow point. The measured tangential drag was very sensitive to small increases in angles at all tow speeds. The ratio of cylinder length to momentum thickness is shown to collapse the tangential drag coefficients for varying tow angles. The effects of the crossflow resulting from the small angles of tow are shown to have a significant effect on the tangential drag coefficient values. A scaling for the orthogonal force on the cylinders was determined and provides a correction to published normal drag coefficient values for pure crossflow. The presence of the axial turbulent boundary layer has a significant effect on these forces.				
14. SUBJECT TERMS Axial Flow on Cylinders    Cylindrical Turbulent Boundary Layers    Drag Measurements    Tow Tanks				15. NUMBER OF PAGES 29
				16. PRICE CODE
17. SECURITY CLASSIFICATION OF REPORT Unclassified	18. SECURITY CLASSIFICATION OF THIS PAGE Unclassified	19. SECURITY CLASSIFICATION OF ABSTRACT Unclassified	20. LIMITATION OF ABSTRACT  SAR	

## TABLE OF CONTENTS

Section	Page
LIST OF TABLES.....	ii
LIST OF SYMBOLS .....	ii
1 INTRODUCTION .....	1
2 DESCRIPTION OF EXPERIMENTS .....	3
2.1 Test Environment.....	3
2.2 Test Setup.....	4
2.3 Test Methodology .....	6
2.3.1 Fluid Forces .....	6
2.3.2 Momentum Thickness.....	9
3 RESULTS OF EXPERIMENTS .....	13
3.1 Wall Shear Force and Momentum Thickness.....	13
3.2 Orthogonal Force .....	19
4 SUMMARY .....	23
5 REFERENCES .....	25

## LIST OF ILLUSTRATIONS

Figure	Page
1 Cross-Sectional Schematic of Carriage Number 5 and the Towing Basin.....	3
2 Schematic of the Towing Configuration .....	4
3 Solid Model of the Tow Point Design.....	4
4 Digital Photo of an Aluminum Cylinder Towed at 13 m/s .....	5
5 Free-Body Diagram of a Cylinder Towed in a Critical Angle Configuration.....	6
6 Cross-Sectional View of Cylinder.....	7
7 Control Volume for a Cylinder at an Angle to the Tow Direction.....	10
8 Total Measured Drag Versus Tow Speed and Angle of Attack .....	13
9a Shear Force as a Function of Tow Angle .....	13
9b Shear Force as a Function of Tow Speed.....	14
10 Mean Wall Shear Stress as a Function of Tow Angle.....	14
11 Tangential Drag Coefficient as a Function of Tow Angle .....	15
12 Momentum Thickness at the End of the Cylinder as a Function of Tow Angle .....	15
13 Nondimensional Scaling for Drag Coefficient.....	16
14 Tangential Drag Coefficient as a Function of Tow Speed .....	17

## LIST OF ILLUSTRATIONS (Cont'd)

Figure		Page
15	Nondimensional Friction Velocity as a Function of Reynolds Number.....	17
16	Ratio of Outer- to Inner-Length Scales as a Function of Reynolds Number.....	18
17	Mean Wall Shear Stress as a Function of Length Reynolds Number.....	19
18	Orthogonal Drag Coefficient as a Function of Diameter Reynolds Number.....	20
19	Orthogonal Drag Force as a Function of Tow Speed .....	20
20	Orthogonal Drag Force Normalized with Shear Force.....	21

## LIST OF TABLES

Table		Page
1	Tow Angles Versus Tow Speeds for the Materials Tested.....	6

## LIST OF SYMBOLS

$a$	Cylinder radius (mm)
$A_s$	Total cylindrical surface area (m <sup>2</sup> )
$\alpha$	Angle of attack (°)
$B$	Tow point location
$\beta, \phi, \gamma$	Coordinates in cross-sectional plane of cylinder
$C_d$	Tangential drag coefficient = $\frac{\tau_w}{\frac{1}{2}\rho U_o^2}$
$C_n$	Orthogonal drag coefficient = $\frac{F_\gamma}{\frac{1}{2}\rho(U_o \sin \alpha)^2 A_s}$
$d$	Cylinder diameter (mm)
$\delta$	Boundary layer thickness (mm)
$F_\gamma$	Orthogonal force (N)
$F_x$	Horizontal drag force (N)

## LIST OF SYMBOLS (Cont'd)

$F_B$	Net body force
$F_y$	Vertical lift force (N)
$L$	Cylinder length (m)
$M_B$	Moment about point B (N-m)
$\nu$	Kinematic viscosity ( $\text{m}^2/\text{s}$ )
$p$	Static pressure ( $\text{N}/\text{m}^2$ )
$P_\beta, P_\gamma$	Pressure force (N)
$\theta$	Momentum thickness (mm)
$\rho$	Fluid density ( $\text{kg}/\text{m}^3$ )
$r$	Radial coordinate (mm)
$R_x, R_y$	Reaction forces at the tow point (N)
$Re_D$	Reynolds number based on diameter = $\frac{U_o \sin(\alpha) d}{\nu}$
$Re_L$	Reynolds number based on length = $\frac{U_o L}{\nu}$
$Re_\theta$	Reynolds number based on momentum thickness = $\frac{U_o \theta}{\nu}$
$S$	Axial shear force (N)
$\sigma$	Circumferential wall shear stress ( $\text{N}/\text{m}^2$ )
$T_\beta, T_\gamma$	Circumferential wall shear force (N)
$\tau_w$	Axial wall shear stress ( $\text{N}/\text{m}^2$ )
$u(r)$	Mean streamwise velocity (m/s)
$u_\tau$	Friction velocity = $\sqrt{\frac{\tau_w}{\rho}}$ (m/s)
$U_o$	Tow speed (m/s)
$W_{net}$	Net weight (N)
$x$	Streamwise coordinate (m)
$\xi$	Axial coordinate (m)
$y$	Vertical coordinate (m)

# DRAG MEASUREMENTS ON LONG, THIN CYLINDERS AT SMALL ANGLES AND HIGH REYNOLDS NUMBERS

## 1. INTRODUCTION

Historically, the problem of axisymmetric turbulent boundary layers that develop on long, thin cylinders at small angles of attack has received much less attention than has the analogous flat-plate problem. The "axisymmetric problem" relates directly to towed sonar arrays in turns, in maneuvers and transient motions, and in cases where arrays experience positive or negative buoyancy in steady-state tows. Existing modeling and resulting real-time towed array shape predictions are limited in accuracy by the uncertainty in the orthogonal and tangential drag coefficient values. The turbulent wall pressure fluctuations, as well as the flow-induced cylinder vibrations for this class of flows, are also of primary importance with regard to self-noise of towed array sonar systems. Willmarth et al.<sup>1</sup> and Bull and Dekkers<sup>2</sup> suggested that significant effects on the turbulent boundary layer structure may occur because of very small angles of attack. This sensitivity to small angles led Willmarth to design a vertical wind tunnel<sup>1</sup> to eliminate cylinder static deflections caused by gravity.

For very long cylinders, the thickness of the boundary layer ( $\delta$ ) in relation to the cylinder radius ( $a$ ), that is,  $\delta/a$ , becomes an additional parameter of importance. Measurements by Cipolla and Keith<sup>3</sup> conducted at the National Aeronautics and Space Administration (NASA) Langley High-Speed Tow Tank, for which  $\delta/a > 100$  and  $L/a > 10,000$  (where  $L$  is cylinder length), established that, compared to flat-plate cases, axisymmetric boundary layers have a significantly higher wall shear stress and a slower spatial growth rate.

Cipolla and Keith<sup>4</sup> investigated zero-pressure gradient turbulent boundary layers developed on cylinders with diameters of 0.61, 0.89, and 2.5 mm and Reynolds numbers of  $10^4 < Re_\theta < 10^5$  and  $10^8 < Re_L < 10^9$ . The results showed that the wall shear stress is significantly higher than that for a comparable flat-plate case and the spatial growth of the boundary layers is lower than that for a comparable flat-plate case. Also, the mean wall shear stress exhibited spatial variations not seen in zero-pressure gradient flat-plate turbulent boundary layers. For example, measurements on towed lines with radius  $a = 0.445$  mm and  $L = 137$  m have shown that the mean wall shear stress increases to a maximum at approximately 50 m from the tow point, decreases to a minimum at 90 m, and then begins to increase again. These length scales are three orders of magnitude larger than the maximum momentum thickness at the end of the line. Assuming the boundary layer thickness is an order of magnitude greater than the momentum thickness (which is correct for flat-plate cases), a length scale of 90 m is two orders of magnitude greater than  $\delta$  for these cases. Typically,  $10\delta$  is considered the maximum length over which boundary layer turbulence displays any significant correlation. These results suggest that a length scale on the order of  $100\delta$  exists to observe this effect. For this diameter (0.89 mm), the effect was found for towing speeds of 3.1, 9.3, and 14.4 m/s, with the minimum shear stress occurring at approximately the same streamwise distance (90 m) for each tow speed.

Furthermore, ongoing stereo particle image velocimetry measurements by Furey et al.<sup>5</sup> for towed lines of the same diameter reveal a decrease in the boundary layer thickness to a minimum value at the same location (90 m) as the minimum in the shear stress. The apparent quasi-periodic behavior in both  $\delta$  and  $\tau_w$  (axial wall shear stress) has never been experimentally observed before. In each of these investigations, the tow angle was less than  $1^\circ$ .<sup>3-5</sup>

In this investigation, the problem of a long, thin cylinder at very small angles to the flow at moderate-to-high Reynolds numbers is considered. This geometry has several applications in which the total drag in the direction of tow is a primary measured quantity. In this research, the analysis is extended to calculate the force along the axis of the cylinder, which is a primary design parameter for towed sonar arrays. This approach allows an evaluation of the growing turbulent boundary layer, which is particularly relevant for cases of small angles of attack. The force orthogonal to the cylinder axis is also calculated and is used to determine a scaling that accounts for the effect of the turbulent boundary layer in the axial direction on this force.

The use of a high-speed towing tank generates length Reynolds numbers and ratios of the outer to inner boundary layer length scales that are directly relevant to undersea towed array applications. This investigation required  $L/a$  to be on the order of 100 and required the length to be large in comparison to relevant turbulent length scales generated. Despite the large size of the facility, the tank depth limits the length of cylinder that can be towed at an angle. Velocity profile measurements were not available at the time of this investigation. A direct measurement of the total drag on long, small-diameter cylinders enables very accurate measurements of the spatially averaged mean wall shear stress. This measurement, combined with measurements of the cylinder angle, leads to a relationship among the measured drag, axial shear force, orthogonal force, cylinder angle, and tow speed. A control volume analysis was used to determine the momentum thickness  $\theta$  at the end of the cylinder from the axial force.



## 2. DESCRIPTION OF EXPERIMENTS

### 2.1 TEST ENVIRONMENT

Towing tests were conducted using carriage number 5 at the Naval Surface Warfare Center (NSWC), Carderock Division, High-Speed Towing Basin (see Schoenherr and Brownell<sup>6</sup> or go to <http://www50.dt.navy.mil/facilities/data/carr5.html> for the specifications of this facility). The High-Speed Towing Basin comprises two adjoining sections: (1) a deep-water section that is 4.9 m deep, 514 m long, and 6.4 m wide and (2) a shallow-water section that is 3 m deep, 356 m long, and 6.4 m wide.

Figure 1 is a cross-sectional schematic of the shallow end of the tow basin. The carriage is propelled by 16 weight-bearing vertical drive wheels and 16 horizontal driving guide wheels. The speed is regulated with an adjustable, direct-current-voltage, automatic feedback, computerized control system. An automatic controller maintains the carriage speed to within  $\pm 0.03$  m/s. The maximum carriage speed is 25.7 m/s (50 knots), and the maximum average acceleration rate is  $0.49 \text{ m/s}^2$ . Additionally, wave-absorber troughs, which dampen standing surface waves generated by the tow strut, extend along the side walls of the tow tank. The freshwater in the tank was at a uniform temperature of  $20.6^\circ\text{C}$ , with a kinematic viscosity of  $1.01 \times 10^{-6} \text{ m}^2/\text{s}$  and a density of  $998 \text{ kg/m}^3$ . No measurable change in the water density and salinity was measured throughout the depth and length of the tank over the duration of the experiments.

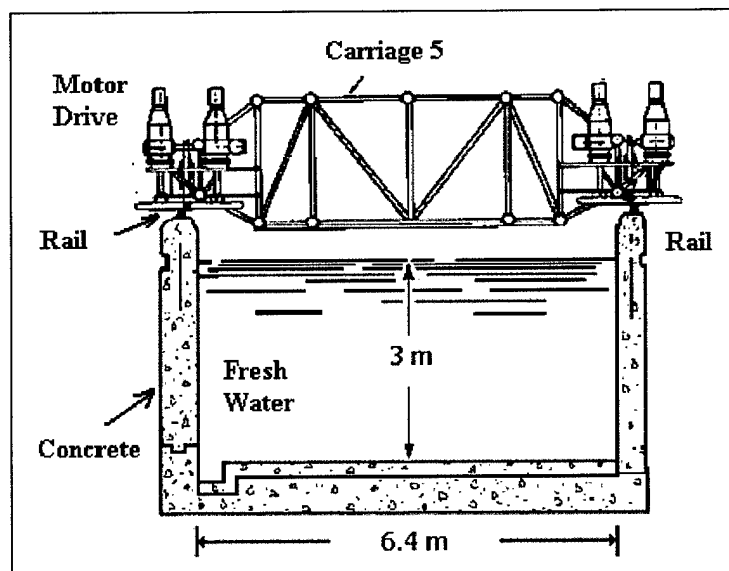


*Figure 1. Cross-Sectional Schematic of Carriage Number 5 and the Towing Basin*

## 2.2 TEST SETUP

The test setup was configured for towing cylinders ( $L = 3.05$  and  $6.10$  m,  $a = 6.35$  mm) at critical angles over a range of speeds in a straight tow configuration, with a simple pinned connection at the tow point. For a particular tow speed, variations in angle were achieved by interchanging cylinders of different densities. This setup, shown in figure 2, eliminated the need for support at the trailing edge, which would cause additional unknown drag forces applied to the load cell. This design also leads to a zero-bending moment at the tow point and load cell and minimizes bending along the length of the cylinder. A cutaway view of the tow point inside the fairing is shown in figure 3.

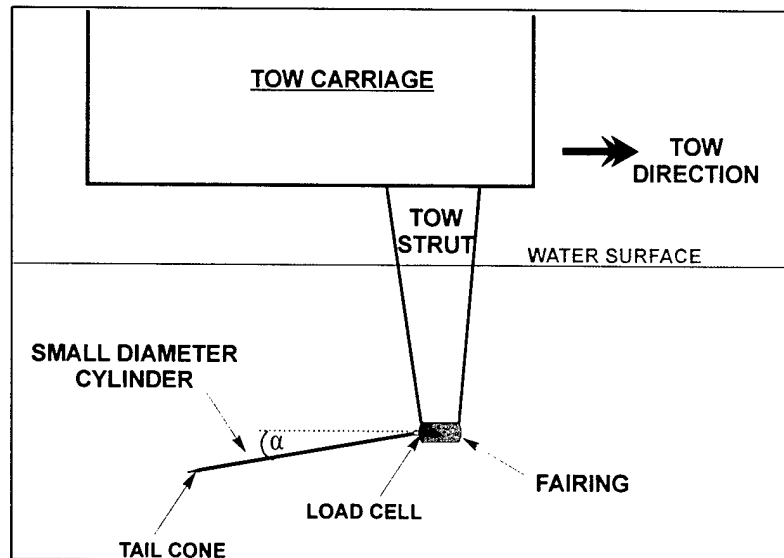


*Figure 2. Schematic of the Towing Configuration*

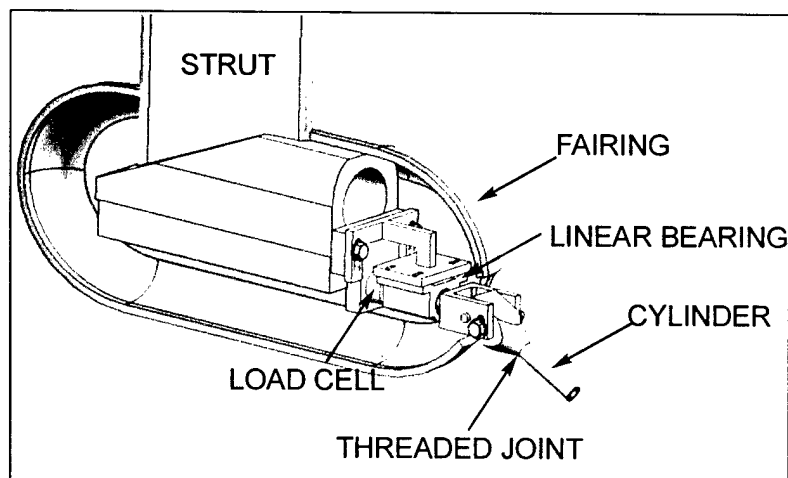


*Figure 3. Solid Model of the Tow Point Design*

The load cell was attached to the base of the towing strut, and a linear bearing was used to support a connecting rod between the load cell and the connecting pin. The fixture was designed to minimize transmission of any vertical force to the load cell and was enclosed in a fiberglass fairing to minimize the generation of turbulence. For each time series of load cell data, the mean value was calculated while the carriage speed was at steady state. This ensemble-averaged force represents the spatially integrated component of force in the tow direction over the surface of the cylinder. For small angles, this force is dominated by the streamwise component of the mean wall shear stress, with an additional component caused by the pressure and circumferential shear forces on the cylinder surface. Because of the large aspect ratios,  $L/a = 480$  and  $960$ , the effects of cylinder base drag were negligible. This result was verified experimentally by repeating drag measurements with and without two different tail cones attached to the cylinder trailing edge. The tail cones were right circular cones with diameters of 12.7 mm and lengths of 76.2 mm and 38.1 mm, respectively. The presence of either cone caused no increase in measured drag with respect to the blunt end case. For each combination of tow speed and tow angle, multiple runs were performed to demonstrate repeatability.

Cylinder tow angles were measured using a Dantec HiSense digital camera, with an 8-bit resolution and a 1280 x 1024-pixel, 60-mm lens. The camera was located in a photography pit, 488 m down the tow tank. A photograph of the aluminum cylinder towed at 13 m/s is shown in figure 4, where the area of each square in the black background grid is  $0.3 \text{ m}^2$ .

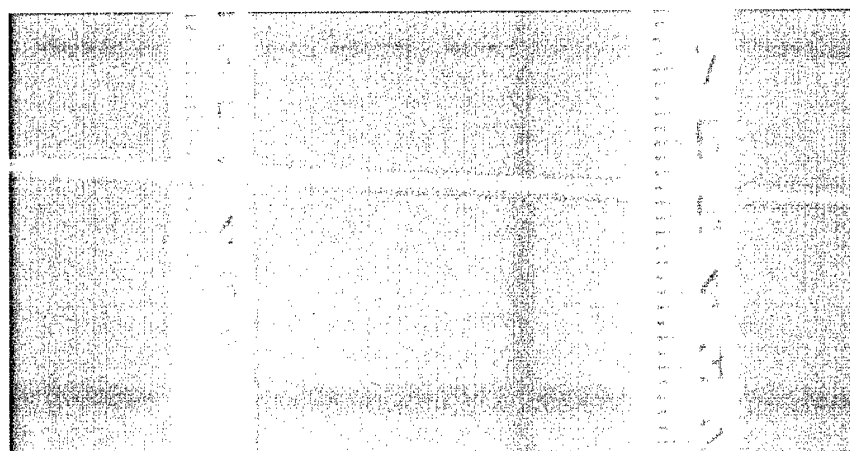


**Figure 4. Digital Photo of an Aluminum Cylinder Towed at 13 m/s**

It was determined from the digital photographs that all cylinders were towed in a linear configuration, with a standard error of less than 5%. The matrix of completed test runs is given in table 1, which lists the cylinder material used to achieve each combination of tow angle and speed.

**Table 1. Tow Angles Versus Tow Speeds for the Materials Tested**

Speed (knots)	Measured Angle (degrees)														
	1.5	2	2.5	3	3.5	4	5	5.5	6	6.5	7	8	9	11	11.5
5									PVC						
10				PVC							AL		Ti		
12										AL		Ti			SS
15		PVC					AL				Ti			SS	
20		PVC			AL			Ti				SS			
25			AL			Ti				SS					
30	PVC		AL	Ti			SS								
35			Ti			SS									
40		Ti													

SS = Stainless Steel, AL = Aluminum, Ti = Titanium, PVC = Polyvinyl Chloride.

## 2.3 TEST METHODOLOGY

### 2.3.1 Fluid Forces

In addition to the two measured quantities  $F_x$  and  $\alpha$ , the fluid forces acting on the cylinder caused by the turbulent flowfield are depicted in figure 5. As shown, these forces are considered to be steady-state values averaged over the length of the cylinder; the tow direction is left to right. The resultant forces are placed at the cylinder's center of mass, which assumes that the forces vary linearly along the length. The error in this assumption is considered negligible because of the slow growth of cylindrical boundary layers found in previous experiments. For the range of angles considered in these experiments ( $\alpha < 12^\circ$ ), the boundary layer was assumed to be attached—but not symmetrical. The xy-coordinate system is moving at a constant velocity equal to the tow speed. Because the cylinder is towed in a critical angle configuration with a pinned connection at B,  $M_B = 0$ .

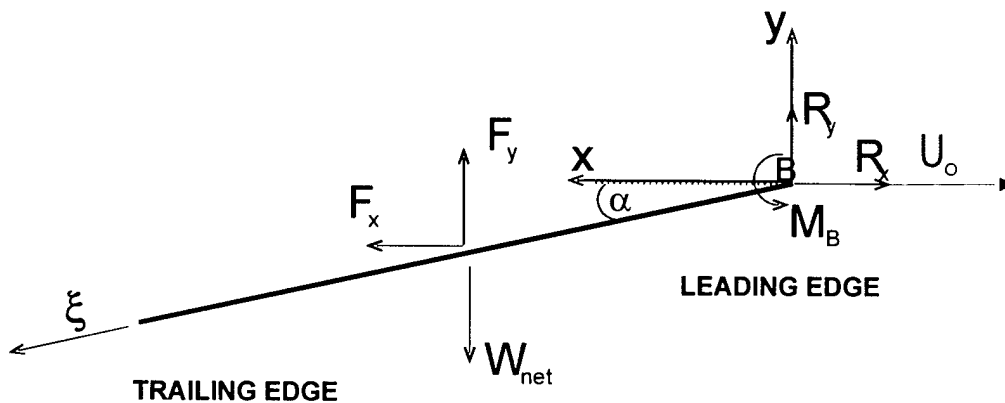


**Figure 5. Free-Body Diagram of a Cylinder Towed in a Critical Angle Configuration**

The objective of the following analysis was to develop an expression for the fundamental boundary layer parameters  $\tau_w$  and  $\theta$  in terms of the measured drag and angle. Figure 6 is a cross-sectional view of the cylinder, normal to the cylinder axis, showing the pressure and circumferential shear stress in that plane.

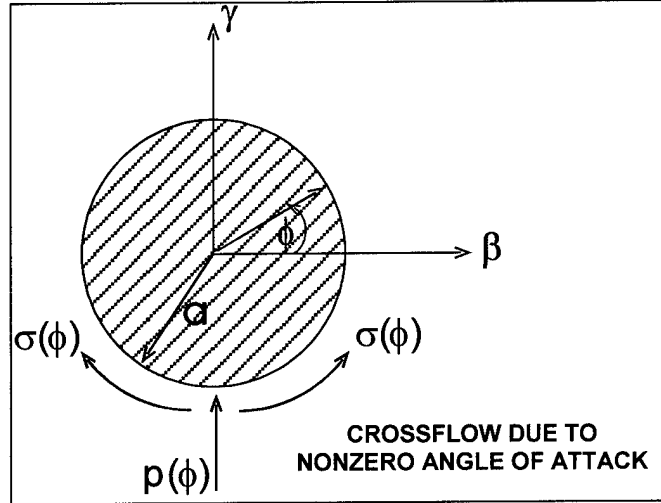


**Figure 6. Cross-Sectional View of Cylinder**

Considering the forces in the  $\beta\gamma$ -plane, the components of pressure force are

$$P_\beta = \int_0^{2\pi} \int_0^L p(\phi) a \cos \phi d\phi d\xi, \quad (1)$$

and

$$P_\gamma = \int_0^{2\pi} \int_0^L p(\phi) a \sin \phi d\phi d\xi. \quad (2)$$

The circumferential wall shear stress also yields force components in the  $\beta$ - and  $\gamma$ -directions:

$$T_\beta = \int_0^{2\pi} \int_0^L \sigma(\phi) a \cos \phi d\phi d\xi, \quad (3)$$

and

$$T_\gamma = \int_0^{2\pi} \int_0^L \sigma(\phi) a \sin \phi d\phi d\xi. \quad (4)$$

Because of the symmetry of the flow (zero yaw angle),  $P_\beta = 0$  and  $T_\beta = 0$ . The forces  $P_\gamma$  and  $T_\gamma$  contribute to the x- and y-components of force shown in figure 5. The force attributed to the wall shear stress in the axial direction is

$$S = \int_0^{2\pi} \int_0^L \tau_w(\phi, \xi) d\phi d\xi. \quad (5)$$

The forces given in equations (2), (4), and (5) comprise the total horizontal and vertical fluid forces acting on the cylinder:

$$F_x = P_\gamma \sin \alpha + T_\gamma \sin \alpha + S \cos \alpha, \quad (6)$$

and

$$F_y = P_\gamma \cos \alpha + T_\gamma \cos \alpha - S \sin \alpha. \quad (7)$$

Static equilibrium defines the reaction forces at the tow point as

$$F_x = R_x, \quad (8)$$

and

$$W_{net} - F_y = R_y. \quad (9)$$

Summing the moments about the tow point  $B$ —assuming a frictionless pin—yields:

$$\sum M_B = 0 = F_y \frac{L}{2} \cos \alpha + F_x \frac{L}{2} \sin \alpha - W_{net} \frac{L}{2} \cos \alpha. \quad (10)$$

Equation (10) simplifies to the following equation:

$$F_y = \frac{W_{net} \cos \alpha - F_x \sin \alpha}{\cos \alpha} = W_{net} - F_x \tan \alpha. \quad (11)$$

Note that all the quantities on the right side of equation (11) are measured. Combining equations (7) and (11), and using equation (6) to eliminate  $(P_\gamma + T_\gamma)$ , gives the following expression for the axial wall shear force:

$$S = \frac{F_x}{\cos \alpha} - W_{net} \sin \alpha. \quad (12)$$

The following expressions for the axial wall shear stress and tangential drag coefficient follow immediately from equation (12):

$$\tau_w = \frac{S}{A_s}, \quad (13)$$

and

$$C_d = \frac{\tau_w}{\frac{1}{2} \rho U_o^2}. \quad (14)$$

This formulation, which gives the shear force tangential to the cylinder, is most relevant to the case of a cylindrical turbulent boundary layer and enables the calculation of the momentum thickness from a control volume analysis, which is analogous to what is stated by Cipolla and Keith<sup>3</sup> and is described in section 2.3.2. In addition, the force along the axis of the cylinder is of primary interest to towed array applications, where the tension in the array is a critical design parameter. This force is also required for dynamic models of towed array shape, in which bending forces within the array are often neglected. Because towed arrays are typically towed at small angles of attack, these experiments are representative of the type of flow experienced in Navy applications, although the cylinders described here have a much smaller aspect ratio ( $L/a$ ).

The total force exerted by the fluid on the cylinder orthogonal to the cylinder axis is composed of the pressure and the circumferential shear forces in the  $\gamma$ -direction:

$$F_\gamma = P_\gamma + T_\gamma. \quad (15)$$

Combining equations (6) and (11) leads to an expression for  $(P_\gamma + T_\gamma)$ :

$$F_\gamma = P_\gamma + T_\gamma = W_{net} \cos \alpha. \quad (16)$$

An orthogonal drag coefficient can then be defined as

$$C_n = \frac{F_\gamma}{\frac{1}{2} \rho (U_o \sin \alpha)^2 A_s}. \quad (17)$$

Note that this coefficient uses the relevant component of velocity,  $U_o \sin \alpha$ , to normalize the force.

### 2.3.2 Momentum Thickness

In figure 7, a cylindrical control volume is defined so that the outer edge is the maximum boundary layer thickness at the end of the cylinder. The axis of the control volume is

coincident with the axis of the cylinder, that is, the  $\xi$ -axis. Note that this layer is an asymmetric boundary layer, so the resulting values of  $\delta$  and momentum thickness  $\theta$  will be average values over the circumference. These values are relevant to towed arrays because the internally mounted hydrophones are not directional and therefore average around the circumference. Furthermore, flow noise models employ average values of the boundary layer parameters at a given axial location. The average momentum thickness can serve as an outer-length scale, and  $\tau_w$  is required for the inner-length scale—which are the relevant length scales for boundary-layer-dominated flows. For cases of larger tow angles, for which the boundary layer separates, the cylinder diameter then becomes a relevant length scale.

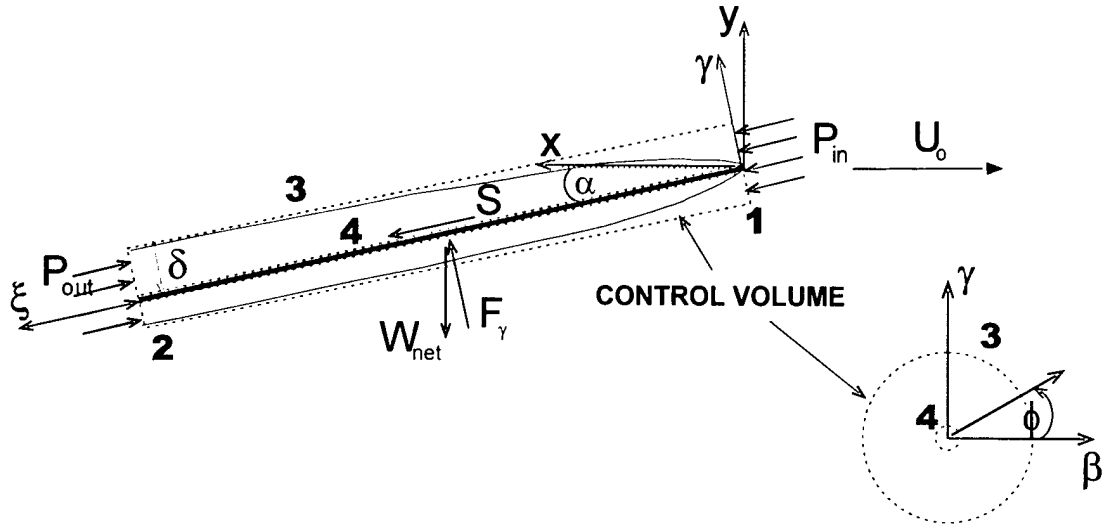


**Figure 7. Control Volume for a Cylinder at an Angle to the Tow Direction**

When considering the forces on the control volume in the  $\xi$ -direction, the only surface force is the shear force  $S$  acting on the wall of the cylinder. Control surfaces 1 and 2 (figure 7) experience different static pressure forces caused by the differences in elevation. This pressure differential is balanced by the component of the net weight in that direction, so that the net body force  $F_B$  is zero. For the case of steady-state flow, the governing equations (conservation of mass and momentum) are

$$\int_{CS} \rho \bar{V} \cdot d\bar{A} = 0, \quad (18)$$

and

$$\int_{CS} u_{\xi} \rho \bar{V} \cdot d\bar{A} = S + F_{B_{\xi}}. \quad (19)$$



Let  $u(r, \phi)$  be the horizontal velocity in the boundary layer at the end of the cylinder. Because the tow direction is at an angle  $\alpha$  to the cylinder axis, the velocity at the inlet to the control volume is  $U_o \cos \alpha$ . There is no flow across control surface 4 (see figure 7), so evaluating equation (18) gives:

$$(U_o - u)A_1 \cos \alpha = (\bar{V} \bullet \bar{A})_3. \quad (20)$$

Using equation (20), equation (19) becomes

$$\frac{S}{\rho(U_o \cos \alpha)^2} = \int_{CS_1} \left[ \frac{u}{U_o} \left( 1 - \frac{u}{U_o} \right) \right] dA_1, \quad (21)$$

where  $dA_1 = r dr d\phi$ . For a cylindrical geometry, the momentum thickness is defined by Cipolla and Keith<sup>3</sup> as

$$\theta^2 + 2a\theta = 2 \int_a^{a+\delta} \left[ \frac{u}{U_o} \left( 1 - \frac{u}{U_o} \right) \right] r dr. \quad (22)$$

Equating the right sides of equations (21) and (22) and then simplifying yields

$$\frac{S}{\pi \rho (U_o \cos \alpha)^2} = \theta^2 + 2a\theta. \quad (23)$$

Since the left side of equation (23) consists of measured quantities, this expression enables evaluation of the momentum thickness at the end of the cylinder.

### 3. RESULTS OF EXPERIMENTS

#### 3.1 WALL SHEAR FORCE AND MOMENTUM THICKNESS

The total measured drag  $F_x$  as a function of tow speed  $U_o$  and angle of attack  $\alpha$  are shown in figure 8 for the four different materials tested. These data were used to calculate the axial wall shear force  $S$  for the four cylinders using equation (12).

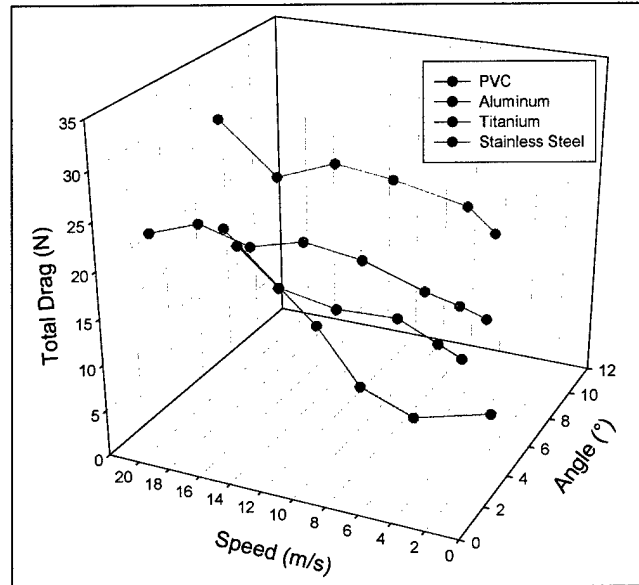


**Figure 8. Total Measured Drag Versus Tow Speed and Angle of Attack**

Figures 9a and 9b show the data plotted as  $S$  versus  $\alpha$  for constant speeds and  $S$  versus  $U_o$  for constant angles of attack. As expected, the shear force for a fixed angle increased with tow speed; however, no clear trend was observed when the angle was varied at a fixed speed.

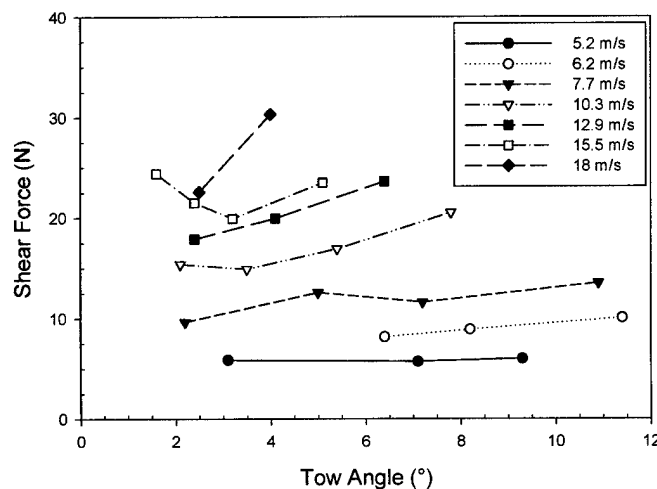


**Figure 9a. Shear Force as a Function of Tow Angle**

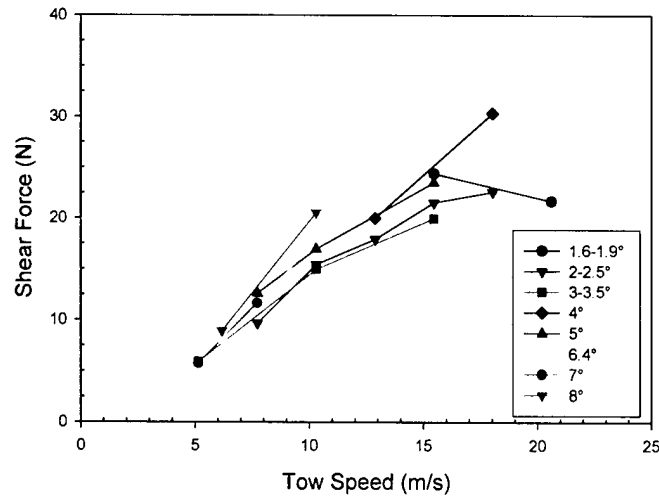


**Figure 9b. Shear Force as a Function of Tow Speed**

The axial wall shear stress  $\tau_w$  and the tangential drag coefficient  $C_d$  were calculated from the shear force  $S$  using equations (13) and (14). In defining  $C_d$ , the tow speed  $U_o$ , rather than the axial component  $U_o \cos \alpha$ , was used. Figure 10 shows  $\tau_w$  versus  $\alpha$  for all combinations of tow speed and angle. Recall that the wall shear stress has been averaged over the entire surface area of the cylinder (circumference and length), so that details of the boundary layer asymmetry are not identified. The different colors denote angles that are similar, and the symbols denote equivalent tow speeds.

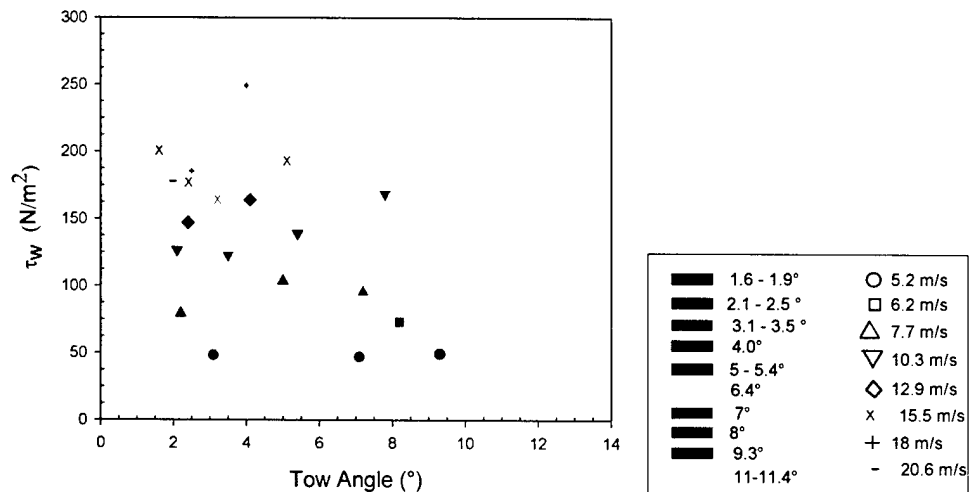


**Figure 10. Mean Wall Shear Stress as a Function of Tow Angle**

Nondimensionalizing  $\tau_w$  to obtain  $C_d$ , as shown in figure 11, leads to a clear trend of decreasing values of  $C_d$  with increasing speed over the range of angles. Each data set is for constant speed, except for the data obtained with the 6.10-m-long cylinder, which was towed at three different speeds. A large variation in  $C_d$  was measured depending on the value of  $U_o$ . Also, at a given speed,  $C_d$  increases with increasing angle. The values of momentum thickness  $\theta(L)$  at the end of the cylinder were calculated using equation (20) and are shown as a function of tow angle in figure 12.

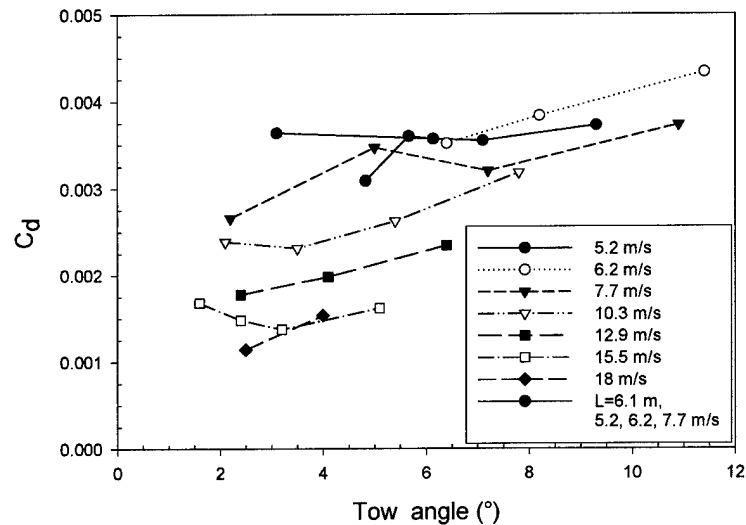


**Figure 11. Tangential Drag Coefficient as a Function of Tow Angle**

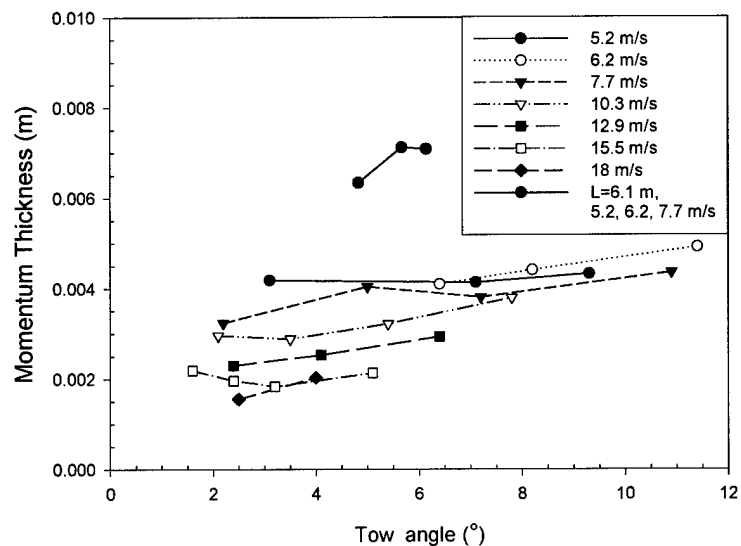


**Figure 12. Momentum Thickness at the End of the Cylinder as a Function of Tow Angle**

The expected trends of increasing  $\theta(L)$  with decreasing tow speed and increasing angle are apparent. This trend indicates that, for a given speed, increasing the tow angle leads to the development of a thicker turbulent boundary layer. The dependence of wall shear stress on angle for a fixed speed is somewhat more complicated (as shown in figure 10). The trend of decreasing mean wall shear stress that would be associated with a thicker flat-plate, zero-pressure-gradient turbulent boundary layer is not apparent and suggests a departure from that ideal case. The momentum thickness values provide an outer-boundary-layer length scale for subsequent data analysis.

To obtain a collapse of the data, the nondimensional quantity  $(L/\theta)^n$  was introduced as a scaling on  $C_d$ , where  $n$  is an empirically determined constant. This scaling introduces the only measured boundary layer outer-length scale, with the ratio  $L/\theta$  serving as an indication of boundary layer growth over the length of the cylinder. The results are shown in figure 13, with  $n = 0.5$ . Included in these results are a limited number of measurements obtained for a 6.1-m cylinder; these measurements collapse with the 3.05-m cylinder data. It is interesting to note that the scaling leads to a linear trend, approaching a nearly constant value of  $C_d (L/\theta)^n$ . Because each quantity was varied independently, this collapse demonstrates that  $L/\theta$  is an appropriate scaling. In addition, it is shown that the cylinder lengths are sufficient to achieve statistically meaningful boundary layer flows in terms of the spatial development.

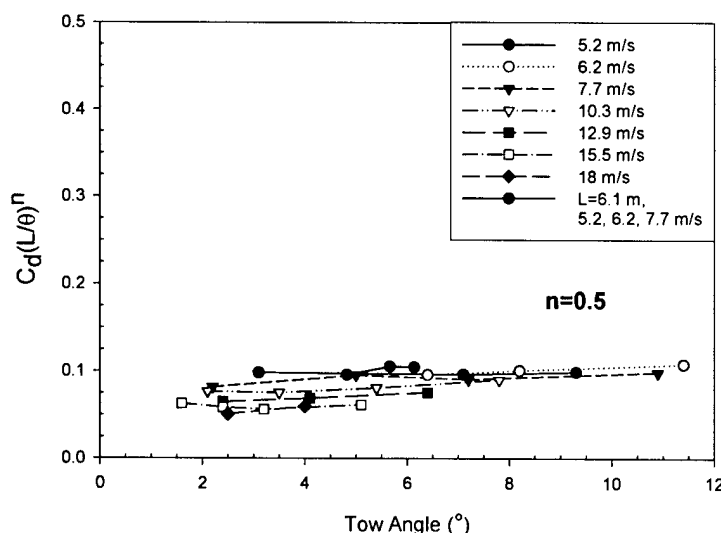


**Figure 13. Nondimensional Scaling for Drag Coefficient**

The data are replotted in figure 14 for data sets of approximately constant values of angle of attack, with  $C_d$  plotted as a function of  $U_o$  for all angles obtained for the 3.05-m-long cylinders. In this form, the data display the expected trend of decreasing  $C_d$  with increasing speed for all angles—although the values are lower than those that flat-plate theory would predict at the highest speeds. The data for different angles follow a similar trend, with the largest angles corresponding to higher values of  $C_d$ . Figure 15 is a plot of  $u_\tau/U_o$  as a function of  $Re_L$ , with data from Coles<sup>7</sup> shown as a solid blue line. In this Reynolds number range, corresponding to  $2 \times 10^4 \leq Re_\theta \leq 5 \times 10^4$ , the quantity  $u_\tau/U_o$  decreases with increasing length Reynolds number for both the cylinder and flat-plate data. The cylinder data highlight the variation of shear stress with small changes in angle at all speeds.

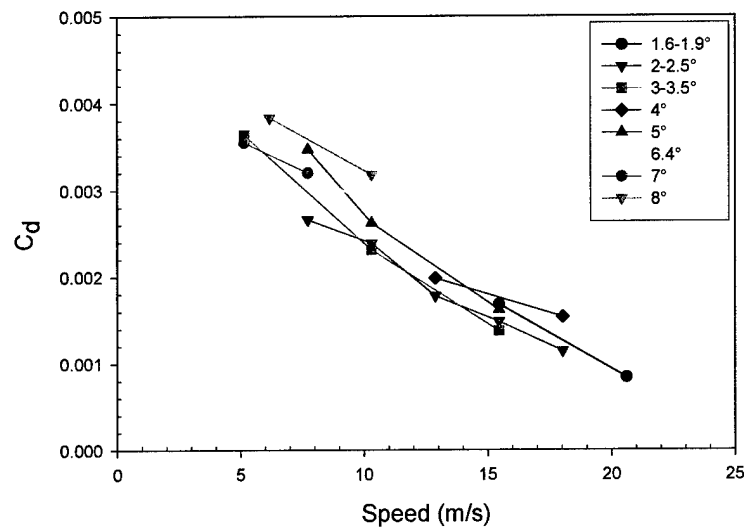


**Figure 14. Tangential Drag Coefficient as a Function of Tow Speed**

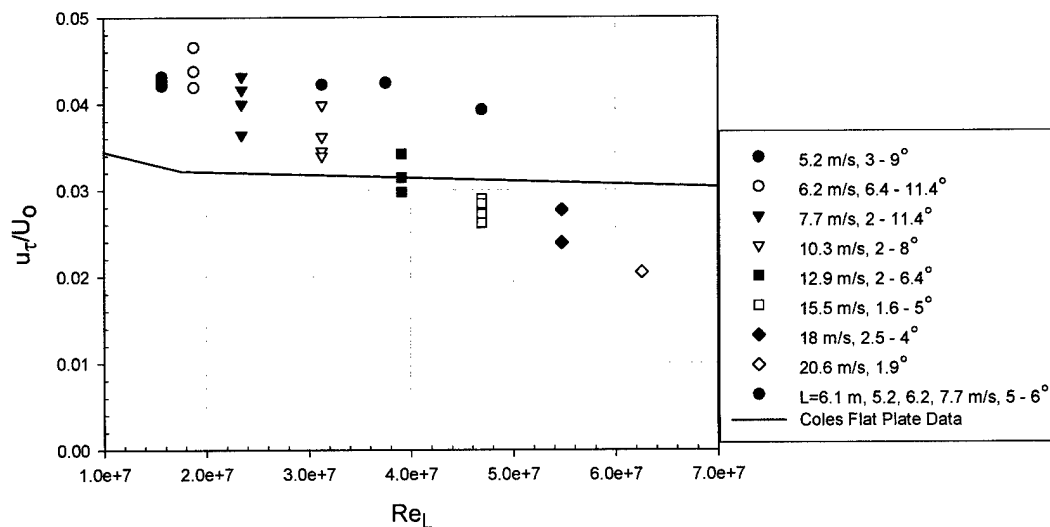


**Figure 15. Nondimensional Friction Velocity as a Function of Reynolds Number**

Although the boundary layers are asymmetric for cases of nonzero angle, they can be characterized by circumferentially averaged inner- and outer-length scales. The ratio of outer-length to inner-length scale values ( $\theta/\nu/u_\tau$ ) is plotted as a function of  $Re_\theta$  in figure 16, along with values for a flat-plate boundary layer taken from Coles.<sup>7</sup> The measured values do not deviate significantly from those for a flat plate, and no clear trend is apparent with speed or angle. This result is expected in terms of the ratio  $\delta/d$ . Assuming that  $\delta$  is an order of magnitude greater than  $\theta$ , the ratio  $\delta/d$  is then of order 1, which is not sufficient for strong curvature effects. In contrast, measurements obtained for higher aspect ratio cylinders<sup>3-5</sup> showed values of  $\theta/\nu/u_\tau$  that were two to three times higher than flat-plate values in this range of Reynolds numbers.

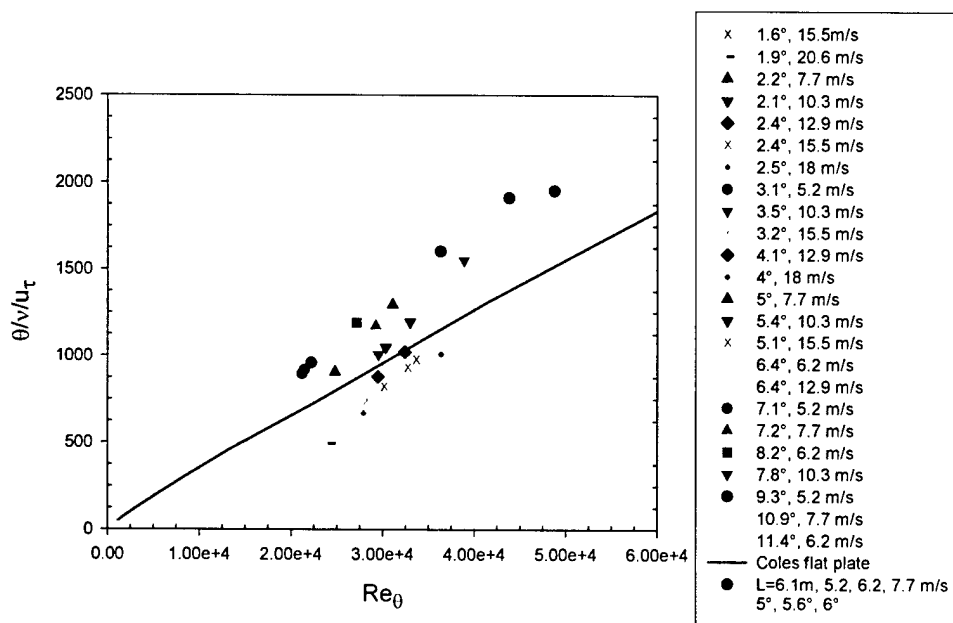
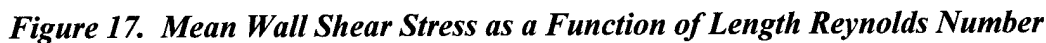


**Figure 16. Ratio of Outer- to Inner-Length Scales as a Function of Reynolds Number**

Figure 17 shows  $\tau_w$  versus length Reynolds number  $Re_L$  for all combinations of tow speed and angle for the 3.05-m cylinders. Also plotted as open circles are the values of the spatially averaged  $\tau_w$  predicted for a flat-plate turbulent boundary layer<sup>8</sup> of the same length at zero angle of attack. Consideration of the variation of  $\tau_w$  as a function of  $U_o L_o/\nu$  facilitates comparison of the measured data with flat-plate boundary layer results. The length scale  $L_o$  can be viewed as a reference length (since data for only one length of cylinder are included) and increasing values of  $U_o L_o/\nu$  are strictly the result of an increase in tow speed. At low speeds, the values of  $\tau_w$  agree with the flat-plate values; however, as  $U_o$  is increased,  $\tau_w$  appears to reach a maximum value and departs significantly from the flat-plate values. This result corresponds to the lower  $C_d$  values shown in figure 12 at high speeds. This behavior was observed for all tested angles of attack, including the smallest value  $\alpha = 1.6^\circ$ .



### 3.2 ORTHOGONAL FORCE

19



$\sin(\alpha)$  term in each quantity. Figure 19 shows the orthogonal drag  $F_\gamma$  as a function of tow speed for approximately constant angles. At a given speed, the orthogonal force on the 3.05-m cylinders increases with increasing angle, as expected; however, the values of  $F_\gamma$  for the 6.1-m cylinder do not vary over the range of angles 4.8 to 6.1°.

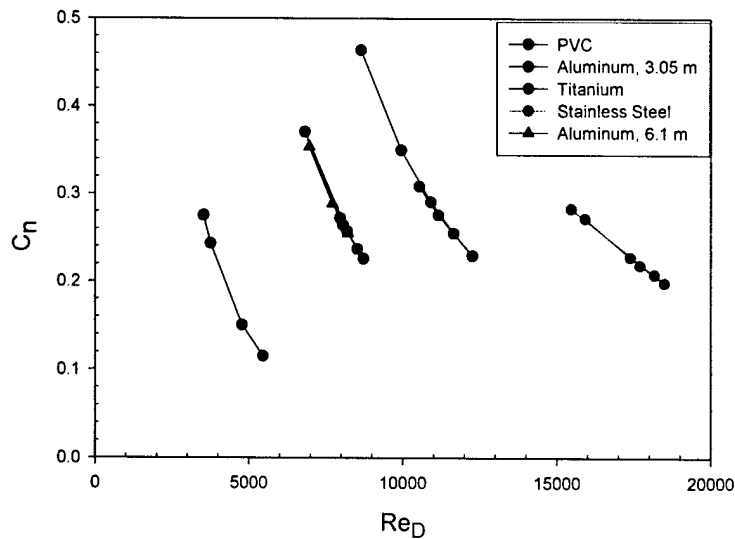


**Figure 18. Orthogonal Drag Coefficient as a Function of Diameter Reynolds Number**

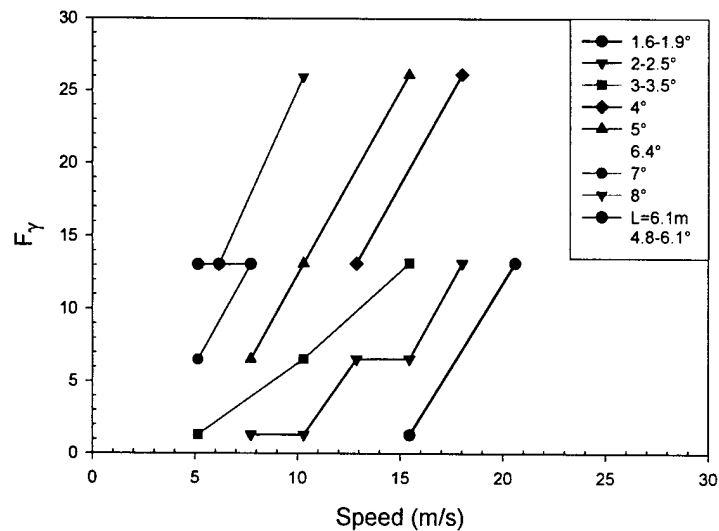


**Figure 19. Orthogonal Drag Force as a Function of Tow Speed**

To collapse the data, scaling is sought for the orthogonal force that takes into account the effect of the turbulent boundary layer in the axial direction. From the data in figure 18, it is apparent that the effect of the boundary layer is to reduce the momentum deficit on the low-pressure side (upper surface) of the cylinders, resulting in a lower crossflow drag. This effect is likely accompanied by a marked change in the vortex shedding with respect to the case of simple flow past a cylinder without the presence of an axial boundary layer. An inner variable scaling for the boundary layer is taken to reflect the changes in the crossflow vortex shedding; therefore, the force  $F_y$  is normalized by the corresponding measured axial shear force values, the results of which are shown in figure 20. The term  $U_o \sin \alpha / u_\tau$  represents a Reynolds number based on the viscous length  $\nu / u_\tau$ . The results show that this scaling collapses all data over the range of Reynolds numbers, tow angles, and lengths. Although additional measurements are required to refine this scaling, this analysis provides a simple method to estimate the orthogonal force from the tension (average shear force) and local angle. This approach can be used to improve models of array shape that currently use a single average value for the crossflow drag coefficient for all angles and speeds.

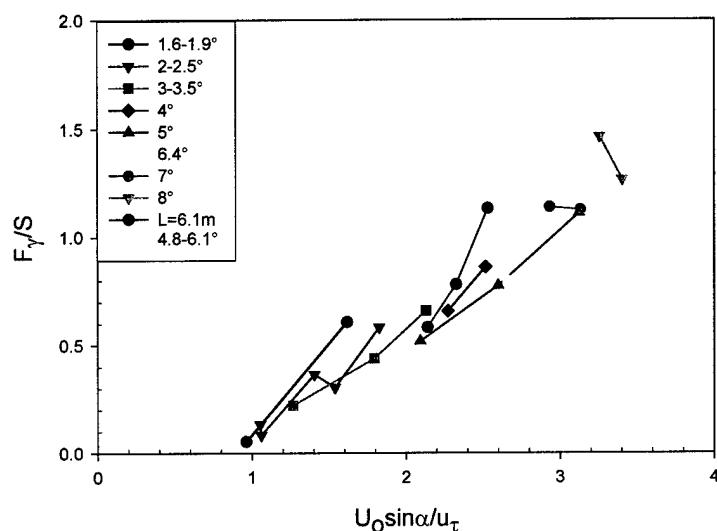


**Figure 20. Orthogonal Drag Force Normalized with Shear Force**

#### 4. SUMMARY

Direct drag measurements on long, small-diameter towed cylinders at small angles of attack and high Reynolds numbers were performed in the High-Speed Towing Basin at the Naval Surface Warfare Center. The primary purpose of this investigation was to determine the sensitivity of the tangential drag force to small angles for a long, slender cylinder under tow. The use of a high-speed tow tank enables development of very high Reynolds number turbulent boundary layers without interference from the walls. The inherent design of the experiment precluded an independent variation of angle and tow speed. The facility itself limited the maximum tow angle and the minimum Reynolds numbers that could be achieved. Nevertheless, a wide range of parameter values was covered during these experiments. The temporal and spatial mean wall shear stress along the cylinder surface was computed from the measured drag, and the data deviated significantly from flat-plate boundary layer data. The tangential drag coefficient was found to be very sensitive to small changes in tow angle at a given speed. The ratio of cylinder length to maximum momentum thickness was used to collapse the data for all angles and tow speeds.

As tow speed was increased, the value of  $\tau_w$  increased to a maximum and then decreased at higher speeds for all angles. This trend points to a true Reynolds number effect, and detailed turbulence measurements are required to determine the alteration of the boundary layer structure. The trend of increasing momentum thickness  $\theta(L)$  with decreasing tow speed and increasing angle was found. At a fixed speed, increasing the tow angle led to the development of a thicker turbulent boundary layer. From these measurements, the detailed structure of the asymmetric boundary layer are unknown, as are the variation of  $\tau_w$  and  $\theta$  along the length of the cylinder. The force orthogonal to the cylinder was also computed from the data and was found to be sensitive to tow angle and speed. The related orthogonal drag coefficient is significantly lower than values for cylinders in pure crossflow. The measured axial shear force was used to normalize the orthogonal force and to collapse the data for all angles and tow speeds. Additional experiments using cylinders of additional lengths and diameters are required to further refine the scaling laws for orthogonal force and tangential drag coefficient.

The results of these experiments confirm that simple corrections to drag forces using components of flow based on geometry are insufficient. The sensitivity of cylindrical boundary layers to small changes in angle of attack agrees with the findings of Willmarth et al.<sup>1</sup> For towed array shape modeling, these results show that applying flat-plate theory to determine the values of the tangential drag coefficients will lead to significant errors. Assumptions for the orthogonal drag based on simple crossflow, without the presence of a boundary layer, are also inadequate. While the geometries investigated in this research represent a small subset of those encountered in towed array maneuvering, they establish a set of baseline measurements for this class of problems. Future studies should address additional values of tow angle and non-zero yaw angles, with the focus on the effect of the turbulent boundary layer on this class of flows.

## 5. REFERENCES

1. W. W. Willmarth, L. K. Sharma, and S. Inglis, "The Effect of Cross Flow and Isolated Roughness Elements on the Boundary Layer and Wall Pressure Fluctuations on Circular Cylinders," Report No. 014439-01, Department of Aerospace Engineering, University of Michigan, January 1977.
2. M. K. Bull and W. A. Dekkers, "Vortex Shedding from Long Slender Cylinders in Near-Axial Flow," *Physics of Fluids A*, vol. 5, no. 12, 1993, pp. 3296-3298.
3. K. M. Cipolla and W. L. Keith, "Momentum Thickness Measurements for Thick Axisymmetric Turbulent Boundary Layers," *Journal of Fluids Engineering*, vol. 125, 2003, pp. 569-575.
4. K. M. Cipolla and W. L. Keith, "High Reynolds Number Thick Axisymmetric Turbulent Boundary Layer Measurements," *Experiments in Fluids*, vol. 35, no. 5, 2003, pp. 477-485.
5. D. A. Furey, K. M. Cipolla, and P. Atsavapranee, "Investigation of the Turbulent Boundary Layer Flow on a Microfilament Array," *Proceedings of the 25th Symposium on Naval Hydrodynamics*, August 2004.
6. K. E. Schoenherr and W. F. Brownell, "The High-Speed Basin and Instrumentation at the David Taylor Model Basin," DTMB Report 1660, David Taylor Model Basin (now the Naval Surface Warfare Center), Carderock, MD, January 1963.
7. D. Coles, "Measurements in the Boundary Layer on a Smooth Flat Plate in Supersonic Flow, Pt. 1. The Problem of the Turbulent Boundary Layer," Technical Report No. 20-69, Jet Propulsion Laboratory, California Institute of Technology, Pasadena, CA, 1 June 1953.
8. H. Schlichting, *Boundary-Layer Theory*, 7th edition, McGraw-Hill, New York, 1979, pp. 635-667.
9. J. O. Hinze, *Turbulence*, 2nd edition, McGraw-Hill, New York, 1975, pp. 683.
10. F. M. White, *Viscous Fluid Flow*, McGraw-Hill, New York, 1974, pp. 207.

## INITIAL DISTRIBUTION LIST

Addressee	No. of Copies
Office of Naval Research (ONR-321MS (M. Traweek, J. McEachern), ONR-333 (R. Joslin))	3
Naval Sea Systems Command (PMS-4011T (S. Greenberg))	1
Defense Technical Information Center	2
Center for Naval Analyses	1
Naval Surface Warfare Center Carderock (Code 5300 (D. Furey (5)), Code 5600 (P. Atsavapranee (1)), Code 00 (J. Barkyoumb (1)), Code 725 (T. Farabee (1)), Code 725 (M. Goody (1)))	9
Applied Physical Sciences Corp. (B. Abraham)	1
U.S. Coast Guard Academy (CDR K. Colella)	1
Rutgers University (T. Wei)	1
NASA Langley Research Center (D. Bushnell)	1
The College of New Jersey (L. Grega)	1